Spectroscopic characterization of highly doped ZnO films grown by atomic-layer deposition for three-dimensional infrared metamaterials [Invited]

Andreas Frölich[*] and Martin Wegener

DFG-Center for Functional Nanostructures (CFN), Institut für Angewandte Physik, and Institut für Nanotechnologie, Karlsruhe Institute of Technology (KIT), D-76128 Karlsruhe, Germany
*Andreas.froelich@kit.edu

Abstract: We systematically study the optical spectra of ZnO grown by atomic-layer deposition as a function of Al (and Ti) doping concentration. The spectra measured on films are well described by fits using a Drude free-electron model. The derived plasma frequencies are consistent with the expected amount of doping and can be continuously and controllably tuned from small values to about 400 THz. The losses (damping) are also quantified. In addition, we achieve smooth conformal coatings of three-dimensional polymer templates made by direct laser writing. Altogether, Al:ZnO appears as an attractive "tunable metal" for three-dimensional infrared metamaterials or transformation-optics architectures.

References and links

1. P. R. West, S. Ishii, G. V. Naik, N. K. Emani, V. M. Shalaev, and A. Boltasseva, "Searching for better plasmonic materials," Laser Photonics Rev. **4**(6), 795–808 (2010).
2. A. Boltasseva and H. A. Atwater, "Low-loss plasmonic metamaterials," Science **331**(6015), 290–291 (2011).
3. X. Yu, Y.-J. Lee, R. Furstenberg, J. O. White, and P. V. Braun, "Filling fraction dependent properties of inverse opal metallic photonic crystals," Adv. Mater. **19**(13), 1689–1692 (2007).
4. J. K. Gansel, M. Thiel, M. S. Rill, M. Decker, K. Bade, V. Saile, G. von Freymann, S. Linden, and M. Wegener, "Gold helix photonic metamaterial as broadband circular polarizer," Science **325**(5947), 1513–1515 (2009).
5. F. Formanek, N. Takeyasu, T. Tanaka, K. Chiyoda, A. Ishikawa, and S. Kawata, "Three-dimensional fabrication of metallic nanostructures over large areas by two-photon polymerization," Opt. Express **14**(2), 800–809 (2006).
6. J. Li, M. M. Hossain, B. Jia, D. Buso, and M. Gu, "Three-dimensional hybrid photonic crystals merged with localized plasmon resonances," Opt. Express **18**(5), 4491–4498 (2010).
7. R. Malureanu, A. Alabastri, W. Cheng, R. Kiyan, B. Chichkov, A. Andryieuski, and A. Lavrinenko, "Enhanced broadband optical transmission in metallized woodpiles," Appl. Phys. A **103**(3), 749–753 (2011).
8. A. Radke, T. Gissibl, T. Klotzbücher, P. V. Braun, and H. Giessen, "Three-dimensional bichiral plasmonic crystals fabricated by direct laser writing and electroless silver plating," Adv. Mater. **23**(17), 3018–3021 (2011).
9. J. S. King, E. Graugnard, O. M. Roche, D. N. Sharp, J. Scrimgeour, R. G. Denning, A. J. Turberfield, and C. J. Summers, "Infiltration and inversion of holographically defined polymer photonic crystal templates by atomic layer deposition," Adv. Mater. **18**(12), 1561–1565 (2006).
10. N. Tétreault, G. von Freymann, M. Deubel, M. Hermatschweiler, F. Pérez-Willard, S. John, M. Wegener, and G. A. Ozin, "New route to three-dimensional photonic bandgap materials: silicon double inversion of polymer templates," Adv. Mater. **18**(4), 457–460 (2006).
11. M. S. Rill, C. Plet, M. Thiel, I. Staude, G. von Freymann, S. Linden, and M. Wegener, "Photonic metamaterials by direct laser writing and silver chemical vapour deposition," Nat. Mater. **7**(7), 543–546 (2008).
12. I. Staude, G. von Freymann, S. Essig, K. Busch, and M. Wegener, "Waveguides in three-dimensional photonic-bandgap materials by direct laser writing and silicon double inversion," Opt. Lett. **36**(1), 67–69 (2011).
13. B. S. Lim, A. Rahtu, and R. G. Gordon, "Atomic layer deposition of transition metals," Nat. Mater. **2**(11), 749–754 (2003).
14. A. Niskanen, T. Hatanpää, K. Arstila, M. Leskelä, and M. Ritala, "Radical-enhanced atomic layer deposition of silver thin films using phosphine-adducted silver carboxylates," Chem. Vap. Deposition. **13**(8), 408–413 (2007).
15. C. E. Kriegler, M. S. Rill, M. Thiel, E. Müller, S. Essig, A. Frölich, G. Freymann, S. Linden, D. Gerthsen, H. Hahn, K. Busch, and M. Wegener, "Transition between corrugated metal films and split-ring-resonator arrays," Appl. Phys. B **96**(4), 749–755 (2009).

16. M. Kariniemi, J. Niinistö, T. Hatanpää, M. Kemell, T. Sajavaara, M. Ritala, and M. Leskelä, "Plasma-enhanced atomic layer deposition of silver thin films," Chem. Mater. **23**(11), 2901–2907 (2011).
17. V. Lujala, J. Skarp, M. Tammenmaa, and T. Suntola, "Atomic layer epitaxy growth of doped zinc oxide thin films from organometals," Appl. Surf. Sci. **82–83**, 34–40 (1994).
18. M. Scharrer, X. Wu, A. Yamilov, H. Cao, and R. P. H. Chang, "Fabrication of inverted opal ZnO photonic crystals by atomic layer deposition," Appl. Phys. Lett. **86**(15), 151113 (2005).
19. J. W. Elam and S. M. George, "Growth of ZnO/Al$_2$O$_3$ alloy films using atomic layer deposition techniques," Chem. Mater. **15**(4), 1020–1028 (2003).
20. S. J. Kwon, "Effect of precursor-pulse on properties of Al-doped ZnO films grown by atomic layer deposition," Jpn. J. Appl. Phys. **44**(2), 1062–1066 (2005).
21. K.-S. An, W. Cho, B. K. Lee, S. S. Lee, and C. G. Kim, "Atomic layer deposition of undoped and Al-doped ZnO thin films using the Zn alkoxide precursor methylzinc isopropoxide," J. Nanosci. Nanotechnol. **8**(9), 4856–4859 (2008).
22. C. H. Ahn, H. Kim, and H. K. Cho, "Deposition of Al doped ZnO layers with various electrical types by atomic layer deposition," Thin Solid Films **519**(2), 747–750 (2010).
23. J. Y. Kim, Y.-J. Choi, H.-H. Park, S. Golledge, and D. C. Johnson, "Effective atomic layer deposition procedure for Al-dopant distribution in ZnO thin films," J. Vac. Sci. Technol. A **28**(5), 1111–1114 (2010).
24. J.-S. Na, G. Scarel, and G. N. Parsons, "In situ analysis of dopant incorporation, activation, and film growth during thin film ZnO and ZnO:Al atomic layer deposition," J. Phys. Chem. C **114**(1), 383–388 (2010).
25. P. Banerjee, W.-J. Lee, K.-R. Bae, S. B. Lee, and G. W. Rubloff, "Structural, electrical, and optical properties of atomic layer deposition Al-doped ZnO films," J. Appl. Phys. **108**(4), 043504 (2010).
26. G. Luka, L. Wachnicki, B. S. Witkowski, T. A. Krajewski, R. Jakiela, E. Guziewicz, and M. Godlewski, "The uniformity of Al distribution in aluminum-doped zinc oxide films grown by atomic layer deposition," Mater. Sci. Eng. B **176**(3), 237–241 (2011).
27. S. Keun Kim, C. Seong Hwang, S.-H. Ko Park, and S. Jin Yun, "Comparison between ZnO films grown by atomic layer deposition using H2O or O3 as oxidant," Thin Solid Films **478**(1-2), 103–108 (2005).
28. G. V. Naik, A. Boltasseva, "A comparative study of semiconductor-based plasmonic metamaterials," Metamaterials **5**(1), 1–7 (2011).

1. Introduction

Most metamaterials contain metals as a crucial ingredient for obtaining their unusual effective optical properties. At optical frequencies, so far, mainly gold or silver have been used in planar electron-beam-lithography processes. However, the large plasma frequency of these noble metals in the range of 2000 THz is not necessarily an advantage for many applications. In particular, one often does not want the real part of the metal electric permittivity to be too far below zero. Ideally, the plasma frequency should be adjustable. Recently, [1,2] have systematically screened and discussed various corresponding options including evaporated highly doped semiconductors or isolators. From this study, Al:ZnO (sometimes also referred to as "AZO") has emerged as one interesting choice because of its small imaginary part of the dielectric function that makes it attractive for example for applications in transformation optics at (near-)infrared wavelengths.

As we show in this work, using such doped materials can also offer interesting perspectives for the fabrication of three-dimensional (3D) metamaterial structures from 3D polymer templates for which evaporation or sputtering cannot be used. For 3D structures, these planar or 2D deposition techniques have to be replaced by 3D infilling or coating techniques, *e.g.*, liquid-based approaches like electroplating [3,4] and electroless deposition [5–8] or gas-based techniques like atomic-layer deposition (ALD) [9] and chemical-vapor deposition (CVD) [10–12]. Regarding ALD and CVD, in addition to the already mentioned conceptual disadvantages of noble metals with respect to certain applications, deposition of smooth, conformal high-quality gold or silver films is not an easy task at all [13–16]. In contrast, ALD of dielectrics such as ZnO is a fairly well established technology that reproducibly leads to smooth thin films for conformal coating of complex 3D scaffolds [17,18]. Even highly doped ZnO films have been deposited [17,19–26]; however, no detailed optical spectroscopic characterization leading to estimates of effective Drude free-electron parameters has been published.

In this paper, we deposit ZnO that is highly doped at variable density with either Ti or Al *via* ALD on flat surfaces. The resulting high-quality smooth, thin films are optically characterized and their effective plasma frequency and damping are derived by comparison with theoretical modeling ("effective-parameter retrieval"). For the highest Al doping

densities, plasma frequencies approaching 400 THz (*i.e.*, only 5 times lower than that of bulk Au) equivalent to a plasma wavelength below 1 µm are achieved. In addition, we deposit on Si wafers and 3D polymer woodpile templates – the drosophila of 3D periodic photonic structures – and demonstrate smooth conformal coating even deep inside the 3D structure.

2. Deposition of doped ZnO films

ALD is a deposition technique based on the sequential and separated exposure of the substrate to the vapors of two (or more) different precursors which both undergo self-terminating reactions with the surface of the growing film. This procedure represents a "single cycle" and leads to the deposition of one monolayer of the material to be deposited. The self-terminating property of the ALD growth technique allows for a precise control of film stoichiometry *via* variation of the precursors introduced into the growth chamber during different cycles.

For the ALD of doped ZnO, we use a commercial ALD apparatus (Savannah 100 by Cambridge Nanotech, Inc.). For pure ZnO, we alternatingly pulse the precursors diethylzinc (DEZ) and H_2O into the reaction chamber. For the Al or Ti doping, an additional trimethylaluminum (TMA) or titaniumisopropoxide (TIP) precursor pulse, respectively, is introduced after N cycles of ZnO. We refer to this sequence of N cycles ZnO and one dopant pulse as a "macro-cycle" (Fig. 1). In this deposition scheme, the nominal doping density can be changed by varying the integer N.
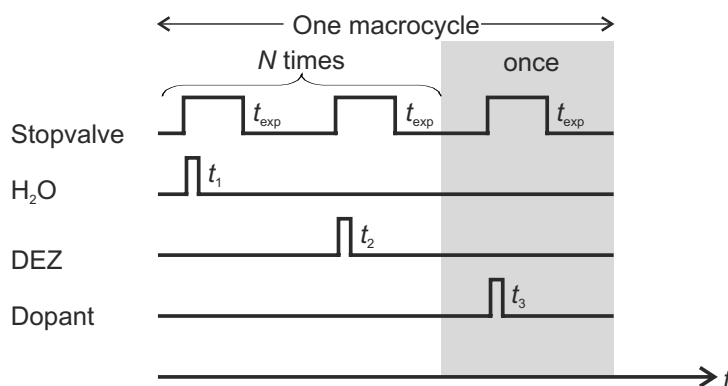

Fig. 1. Pulse sequence used for one macro-cycle of doped ZnO film growth. The vessels containing the precursors are opened for a time t_i (i = 1, 2, 3 - values given below) and the precursor vapors are held in the reaction chamber for a time t_{exp} to allow sufficient time for the precursors to react with the substrate surface by closing the stopvalve between the reaction chamber and the pump. After N cycles of ZnO growth, an additional dopant pulse is introduced into the chamber. $t_1 = t_2 = 15$ ms, whereas $t_3 = 15$ ms for TMA and $t_3 = 0.1$ s for TIP. For the deposition of films on flat substrates we used an exposure time $t_{exp} = 1$ s, whereas we chose an exposure time of $t_{exp} = 5$ s for deposition on three-dimensional substrates. The nominal doping density is controlled by varying the integer N.

Unless noted otherwise, all depositions were carried out under a steady flow of 20 sccm of N_2 and at a substrate temperature of 250 °C. DEZ, TMA and H_2O were evaporated from stainless steel cylinders held at room temperature, the cylinder containing TIP was heated to 80 °C. The number of macro-cycles was chosen such that the resulting films had a thickness on the order of 250 nm. The degree of Al-doping in the film was varied from $N = 72$ to $N = 12$, the degree of Ti-doping from $N = 80$ to $N = 20$.

3. Properties of doped ZnO films deposited by ALD

For the determination of the effective Drude free-electron parameters of the deposited films, we measure intensity transmittance and reflectance spectra at normal incidence using a Fourier-transform infrared (FTIR) spectrometer connected to a microscope. From these spectra, we obtain the effective Drude parameters of the films by fitting them to the calculated

intensity transmittance and reflectance of a slab of material having a thickness d and permittivity

$$\varepsilon(\omega) = \varepsilon_\infty - \frac{\omega_{Pl}^2}{\omega^2 + \gamma^2} + i\frac{\gamma}{\omega}\frac{\omega_{Pl}^2}{\omega^2 + \gamma^2} \tag{1}$$

where ε_∞ is the background permittivity, ω_{Pl} is the (angular) plasma frequency and γ is the collision frequency. ε_∞, ω_{Pl}, γ, and the slab thickness d are used as free parameters for the fit. Figure 2a shows the good agreement between the measured spectra and the best-fit calculation for a film with a nominal doping density given by $N = 27$. The corresponding complex permittivity ε is depicted in Fig. 2b.
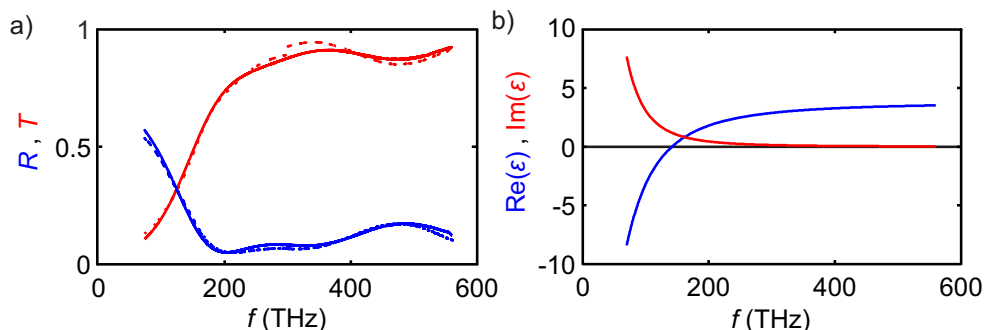

Fig. 2. Optical properties of an Al:ZnO film with a nominal doping density given by $N = 27$. a) Measured intensity reflectance R (blue) and transmittance T (red) spectra under normal incidence (dashed lines) and calculated spectra (solid lines) using the Drude parameters $\varepsilon_\infty = 3.78$, $\omega_{Pl} = 2\pi \cdot 289 \cdot 10^{12}$ s^{-1}, $\gamma = 2\pi \cdot 44 \cdot 10^{12}$ s^{-1} and a slab thickness $d = 253$ nm. An uncoated glass substrate is used as a reference for the transmittance measurements and is also taken into account in the calculations. A silver mirror was used as a reference for reflectance measurements. b) Complex permittivity corresponding to the Drude parameters in a). Results for different values of N are shown in Fig. 3.

We systematically varied the number of ZnO cycles N per dopant cycle, $i.e.$, the nominal dopant concentration, to test whether the plasma frequencies we derive actually originate from the incorporation of dopant atoms into the ZnO film. If this is the case ($i.e.$, if the density of free charges n is inversely proportional to N), we would expect that ω_{Pl} varies proportional to $N^{-1/2}$, considering that the angular plasma frequency predicted by Drude theory is

$$\omega_{Pl}^2 = \frac{ne^2}{\varepsilon_0 m_e^*} \tag{2}$$

where ε_0 is the permittivity of free space, e is the electron charge and m_e^* is the effective electron mass. Our data in Fig. 3 show a clear increase of ω_{Pl} versus $N^{-1/2}$. Ideally, the plasma frequency for a nominally undoped ZnO film corresponding to $N = \infty$ should be zero. However, interpolating our data to $N = \infty$ (dashed line in Fig. 3) we observe an offset that suggests an additional "intrinsic" doping of our films. We attribute this finding to a not-quite stoichiometric composition of the films resulting in a certain background doping independent of N [27]. We could not investigate this further because, unfortunately, at dopant concentrations lower than about $N = 72$, the features in the optical spectra that are indicative of free carriers are outside of the spectral range accessible with our setup.
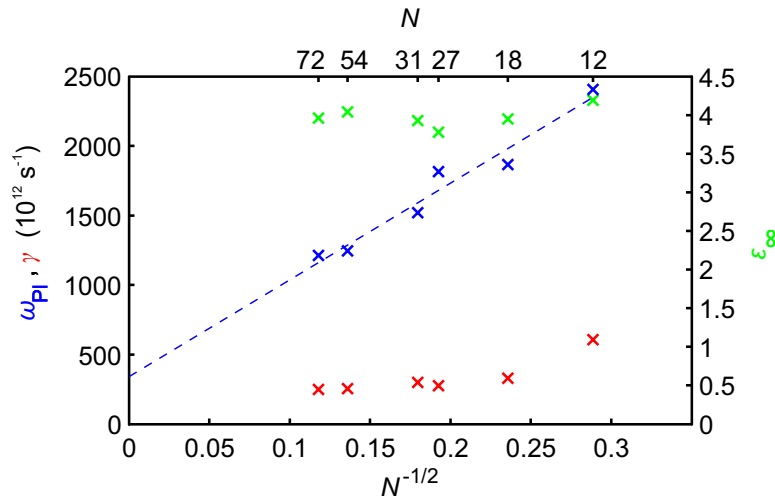
Fig. 3. Dependence of the effective Drude parameters of doped ZnO on the number of ZnO cycles N per dopant pulse. If Al-doping is the only source of free charges, Drude theory predicts that the angular plasma frequency (ω_{Pl}, blue symbols) is proportional to the square root of their density, *i.e.* to $N^{-1/2}$. The lower horizontal axis is chosen to allow for checking this dependence. Obviously, an additional "intrinsic" doping is present in our films. At $N > 72$, a reliable determination of effective parameters is no longer possible with our setup. In addition, we show the collision frequency γ (red symbols) and the background permittivity ε_∞ (green symbols) in Eq. (1). The dashed line is a linear fit to ω_{Pl} and intercepts the *y*-axis at $\omega_{Pl} = 2\pi \cdot 55 \cdot 10^{12}$ s^{-1}.

The derived damping frequencies γ in Fig. 3 reveal a certain increase versus effective doping density. To interpret and compare the resulting imaginary part of the permittivity of our films, we employ a figure-of-merit (FOM) defined as $-\text{Re}(\varepsilon)/\text{Im}(\varepsilon)$. We find that our films exhibit a FOM of 1.13 at a doping level corresponding to $N = 27$ and at operation frequencies between 78 THz and 87 THz. This is somewhat lower than the FOM of 1.8 which has been reported for films fabricated by *planar* pulsed laser deposition in [28]. Reference [1] even anticipates (mainly derived from literature Hall measurements) a FOM of 3 in the near infrared for Al:ZnO. However, parameters derived from Hall and optical measurements, respectively cannot be compared directly, because they correspond to different operating frequencies. We also tested whether the damping frequencies can be reduced by tempering the samples in air at 450 °C for up to 12 h, but we found that this treatment renders the doping less effective, similar to the results in [28].

Importantly, to demonstrate the applicability of our deposition procedure for the realization of *three-dimensional* designs, we deposited 110 nm of Al:ZnO with $N = 18$ as an example on a woodpile photonic-crystal polymer template. To avoid template collapse due to melting of the polymer we chose a substrate temperature of merely 110 °C during the first 12 macro-cycles after which the growing Al:ZnO film is thick enough to protect the template from melting-induced collapse. Figure 4 shows an oblique-view electron micrograph after focused-ion-beam (FIB) milling through the composite structure. Over the entire image the apparent film thickness does not vary by more than 5 nm corresponding to less than 2 times the pixel size, demonstrating conformal coating of the template from its top to its bottom.
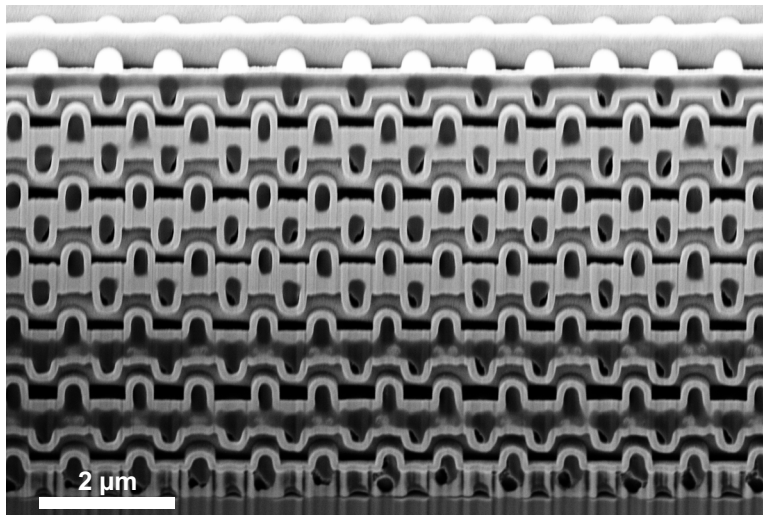
Fig. 4. Oblique-view electron micrograph of a woodpile photonic-crystal polymer template (black to dark gray) coated with Al:ZnO (bright gray) after focused-ion-beam (FIB) milling to reveal the composite's interior. The variation of the Al:ZnO film thickness is less than 5 nm, indicating conformal coating of the structure. The viewing angle is 54° relative to the surface normal.

To further demonstrate the ability of our process to deposit high-quality smooth films, we deposited the same film on a Si wafer as well. Figure 5 shows atomic-force-microscopy (AFM) measurements of the wafer a) before and b) after deposition. The RMS roughness of the uncoated wafer is 0.11 nm and that of the coated wafer is 0.59 nm. This increase indicates a slight roughening due to the ALD process. However, the resulting roughness is much better than, *e.g.*, for silver films fabricated using chemical-vapor deposition (CVD) [15]. The achieved roughness is even competitive with that from very good planar physical-vapor deposition approaches.
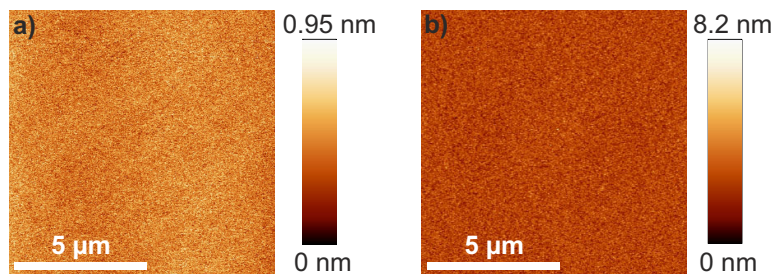

Fig. 5. Atomic-force-microscopy (AFM) images of a Si wafer a) before and b) after deposition of 110 nm of Al:ZnO like in Fig. 4. The resulti RMS roughness of a mere 0.59 nm in b) indicates that very smooth films have been achieved.

For films doped with Ti instead of Al (not depicted), we have also obtained plasma frequencies as large as $2\pi \cdot 185 \cdot 10^{12}$ s^{-1}, but the corresponding damping frequencies of about $2\pi \cdot 60 \cdot 10^{12}$ s^{-1} are significantly larger than those for Al at comparable plasma frequencies. Thus, Al:ZnO is far superior to Ti:ZnO in our experiments.

4. Conclusions

In conclusion, on the basis of our systematic optical spectroscopic characterization, highly Al-doped ZnO grown by atomic-layer deposition onto polymer templates appears as an attractive effective metal for use in three-dimensional infrared metamaterials and complex

transformation-optics architectures. In particular, depositing Al-doped ZnO *via* ALD allows for an easily and continuously adjustable electron density and, hence, free-electron plasma frequency.

Acknowledgments